

# Rare $B_s$ decays in the relativistic quark model

R. N. Faustov and V. O. Galkin

*Dorodnicyn Computing Centre, Russian Academy of Sciences,  
Vavilov Str. 40, 119333 Moscow, Russia*

The branchings fractions of the rare  $B_s$  decays are calculated in the framework of the QCD-motivated relativistic quark model. The form factors of the weak  $B_s$  transitions to light mesons are expressed through the overlap integral of the initial and final meson wave functions in the whole accessible kinematical range. Explicit determination of the momentum transfer dependence of the form factors without additional model assumptions and extrapolations significantly improve the reliability of the obtained results. The approximate analytical form of the form factors is given in order to simplify the comparison with other predictions and experiment. The calculated form factors are applied for the investigations of the rare semileptonic, radiative and nonleptonic  $B_s$  decays. The factorization approximation is used for the description of the nonleptonic decays. All results agree well with available experimental data.

PACS numbers: 13.20.He, 12.39.Ki

## I. INTRODUCTION

The rare weak decays of  $B_s$  mesons are governed by the flavour changing neutral current. In the standard model their description requires calculation of the loop (penguin) diagrams. Thus such decays are very sensitive to the intermediate contributions of the new particles and interactions. The accurate theoretical evaluation and experimental measurement of their decay rates can significantly constrain the “new physics” models.

Theoretical investigation of these rare decays is usually based on the effective Hamiltonian in which intermediate gauge bosons are integrated out. Application of the operator product expansion allows one to separate short- and long-distance effects which are assumed to factorize. The short-distance contributions are described by the Wilson coefficients which are calculated perturbatively. The long-distance part is attributed to the set of the operators, which matrix elements between initial and final meson states are usually parametrized by the set of the invariant form factors. The calculation of these form factors requires application of the nonperturbative methods. Thus the improvement of the theoretical understanding of the rare decays requires the precise control of hadronic uncertainties. The characteristic feature of the rare semileptonic  $B_s$  decays is a very broad kinematical range. Therefore the reliable determination of the momentum transfer dependence of the form factors turn out to be very important. Various theoretical approaches have been applied for the form factor calculations. However, in most of such approaches the decay form factors are determined in some specific kinematic point or interval and then they are extrapolated to the whole kinematical range using some model parametrizations or additional assumptions. Thus in the region of the large recoil of the final meson light-cone QCD sum rules can be applied, while the region of small recoils is accessible to lattice QCD. Most of quark models determine form factors at the single point of zero or maximum recoil and then the Gaussian or pole extrapolations

are applied. Therefore the calculation of the form factors in the whole kinematical range in the framework of the same approach without additional assumptions or/and extrapolations is highly important.

From the experimental side significant progress has been achieved in last years [1–6]. Not only several rare  $B_s$  decays have been observed for the first time and their branching fractions were measured, but also first attempt have been made for measuring the differential branching fraction and longitudinal polarization fraction of the  $\varphi$  meson in the rare semileptonic  $B_s \rightarrow \varphi \mu^+ \mu^-$  decay [2].

In this paper we calculate the rare weak  $B_s$  transition form factors and decay rates in the framework of the relativistic quark model based on the quasipotential approach in quantum chromodynamics (QCD). It was previously successfully applied for evaluating the charmfull and charmless semileptonic  $B_s$  decay form factors [7, 8]. Rare semileptonic decays of  $B$  and  $B_c$  mesons were studied by us in Ref. [9]. This model consistently takes relativistic effects into account. It allows us to express the form factors of the transition matrix elements through the overlap integrals of the meson wave functions. Such expressions are valid in the whole kinematical range and thus do not require additional assumptions or extrapolations. The meson wave functions are known in our model from the previous mass spectra calculations [10, 11]. On the basis of the form factors we then consider the rare semileptonic, radiative and nonleptonic  $B_s$  decays.

The paper is organized as follows. First, in Sec. II we briefly describe our relativistic quark model paying special attention to the method of the calculation of the transition matrix element of the weak current. In Sec. III using this approach we calculate the form factors of the rear weak  $B_s \rightarrow \eta(\varphi)$  transitions. The momentum transfer dependence of the form factors is determined explicitly and the approximate parametrizations of the form factors are given. In Sec. IV these form factors are used for consideration of the rare semileptonic  $B_s \rightarrow \eta(\varphi) l^+ l^-$  decays. The  $B_s \rightarrow \eta(\varphi) \nu \bar{\nu}$  decays are discussed in Sec. V. Section VI contains results for the rare radiative decays. In Sec. VII rare nonleptonic  $B_s$  decays to a charmonium state and a light meson as well as to two light mesons are calculated in the framework of the factorization approximation. All obtained results are confronted with previous predictions and available experimental data. Section VIII contains our conclusions.

## II. RELATIVISTIC QUARK MODEL

### A. Relativistic wave equation and the quasipotential of the quark-antiquark interaction

For further calculations we use the relativistic quark model based on the quasipotential approach in quantum chromodynamics (QCD). In our model hadrons are considered as the bound states of constituent quarks which are described by the single-time wave functions satisfying the three-dimensional relativistically invariant Schrödinger-like equation with the QCD-motivated quark-antiquark potential [12]

$$\left( \frac{b^2(M)}{2\mu_R} - \frac{\mathbf{p}^2}{2\mu_R} \right) \Psi_M(\mathbf{p}) = \int \frac{d^3q}{(2\pi)^3} V(\mathbf{p}, \mathbf{q}; M) \Psi_M(\mathbf{q}), \quad (1)$$

where the relativistic reduced mass is

$$\mu_R = \frac{M^4 - (m_1^2 - m_2^2)^2}{4M^3}, \quad (2)$$

$M$  is the meson mass,  $m_{1,2}$  are the quark masses, and  $\mathbf{p}$  is their relative momentum. In the center of mass system the relative momentum squared on mass shell  $b^2(M)$  is expressed through the meson and quark masses:

$$b^2(M) = \frac{[M^2 - (m_1 + m_2)^2][M^2 - (m_1 - m_2)^2]}{4M^2}. \quad (3)$$

The quark-antiquark quasipotential  $V(\mathbf{p}, \mathbf{q}; M)$  is assumed to be the sum of the perturbative one-gluon exchange term and the nonperturbative confining part [12]

$$V(\mathbf{p}, \mathbf{q}; M) = \bar{u}_1(p)\bar{u}_2(-p)\mathcal{V}(\mathbf{p}, \mathbf{q}; M)u_1(q)u_2(-q), \quad (4)$$

with

$$\mathcal{V}(\mathbf{p}, \mathbf{q}; M) = \frac{4}{3}\alpha_s D_{\mu\nu}(\mathbf{k})\gamma_1^\mu\gamma_2^\nu + V_{\text{conf}}^V(\mathbf{k})\Gamma_1^\mu(\mathbf{k})\Gamma_{2;\mu}(\mathbf{k}) + V_{\text{conf}}^S(\mathbf{k}), \quad \mathbf{k} = \mathbf{p} - \mathbf{q},$$

where  $\alpha_s$  is the QCD coupling constant,  $D_{\mu\nu}$  is the gluon propagator in the Coulomb gauge, and  $\gamma_\mu$  and  $u(p)$  are the Dirac matrices and spinors, respectively. The confining part consists from the Lorentz scalar and vector linearly rising interactions which in the nonrelativistic limit reduce to

$$V_{\text{conf}}(r) = V_{\text{conf}}^S(r) + V_{\text{conf}}^V(r) = Ar + B, \quad (5)$$

with

$$V_{\text{conf}}^V(r) = (1 - \varepsilon)(Ar + B), \quad V_{\text{conf}}^S(r) = \varepsilon(Ar + B), \quad (6)$$

where  $\varepsilon$  is the mixing coefficient. Its value  $\varepsilon = -1$  has been determined from the comparison of the heavy quark expansion for the semileptonic  $B \rightarrow D$  decays in our model [13] with model-independent predictions of heavy quark effective theory and from the consideration of charmonium radiative decays [12]. Note that in the nonrelativistic limit the quasipotential (4) reproduces the well-known Cornell potential. Therefore this quasipotential provides its relativistic generalization.

The long-range vector vertex

$$\Gamma_\mu(\mathbf{k}) = \gamma_\mu + \frac{i\kappa}{2m}\sigma_{\mu\nu}k^\nu \quad (7)$$

contains the Pauli term with anomalous chromomagnetic quark moment  $\kappa$ . The value  $\kappa = -1$  is fixed in our model from the analysis of the fine splitting of heavy quarkonia  $^3P_J$ -states [12] and the heavy quark expansion for semileptonic decays of heavy mesons [13] and baryons [14] and enables vanishing of the spin-dependent chromomagnetic interaction, proportional to  $(1 + \kappa)$ , in accord with the flux tube model.

Other parameters of our model were determined from the previous analysis of meson spectroscopy [12]. The constituent quark masses are  $m_b = 4.88$  GeV,  $m_c = 1.55$  GeV,  $m_s = 0.5$  GeV,  $m_{u,d} = 0.33$  GeV and the parameters of the linear potential are  $A = 0.18$  GeV<sup>2</sup> and  $B = -0.30$  GeV.

## B. Matrix element of the weak current between meson states

The calculation of the branching fractions of rear weak decays requires evaluation of the transition matrix elements of the weak current  $J_\mu^W$  between meson states. In the quasipotential approach such matrix element between a  $B_s$  meson with mass  $M_{B_s}$  and momentum

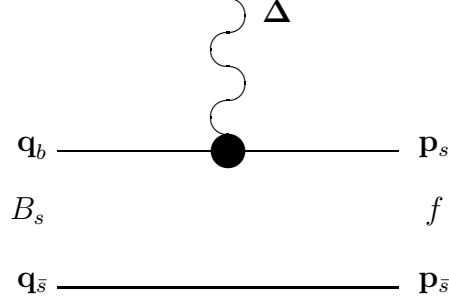


FIG. 1: Leading order vertex function  $\Gamma^{(1)}(\mathbf{p}, \mathbf{q})$ .

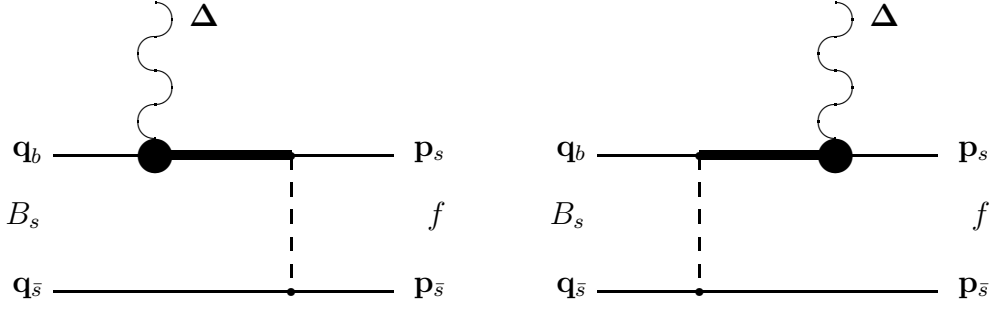


FIG. 2: Subleading order vertex function  $\Gamma^{(2)}(\mathbf{p}, \mathbf{q})$ . Bold lines denote the negative-energy part of the quark propagator. Dashed lines correspond to the exchange by the effective potential  $\mathcal{V}$  (4).

$p_{B_s}$  and a final  $f$  ( $\eta, \eta'$  or  $\varphi$ ) meson with mass  $M_f$  and momentum  $p_f$  is given by [15]

$$\langle f(p_f) | J_\mu^W | B_s(p_{B_s}) \rangle = \int \frac{d^3 p d^3 q}{(2\pi)^6} \bar{\Psi}_{f \mathbf{p}_f}(\mathbf{p}) \Gamma_\mu(\mathbf{p}, \mathbf{q}) \Psi_{B_s \mathbf{p}_{B_s}}(\mathbf{q}), \quad (8)$$

where  $\Gamma_\mu(\mathbf{p}, \mathbf{q})$  is the two-particle vertex function and  $\Psi_{M \mathbf{p}_M}(\mathbf{p})$  are the meson ( $M = B_s, f$ ) wave functions projected onto the positive energy states of quarks and boosted to the moving reference frame with momentum  $\mathbf{p}_M$ , and  $\mathbf{p}, \mathbf{q}$  are relative quark momenta.

The vertex function  $\Gamma_\mu(\mathbf{p}, \mathbf{q})$  contains [7] contributions both from the leading order spectator diagram (Fig. 1) and from subleading order diagrams (Fig. 2) accounting for the contributions of the negative-energy intermediate states. The leading order vertex function

$$\Gamma_\mu^{(1)}(\mathbf{p}, \mathbf{q}) = \bar{u}_s(p_s) J_\mu^W u_b(q_b) (2\pi)^3 \delta(\mathbf{p}_s - \mathbf{q}_s) \quad (9)$$

contains the  $\delta$  function which allows us to take one of the integrals in the matrix element (8) and thus to reduce it to the standard overlap integral of meson wave functions. The subleading order contribution is significantly more complicated

$$\begin{aligned} \Gamma_\mu^{(2)}(\mathbf{p}, \mathbf{q}) = & \bar{u}_s(p_s) \bar{u}_s(p_{\bar{s}}) \left\{ \mathcal{V}(\mathbf{p}_{\bar{s}} - \mathbf{q}_{\bar{s}}) \frac{\Lambda_s^{(-)}(k')}{\epsilon_s(k') + \epsilon_s(q_b)} \gamma_1^0 J_\mu^W \right. \\ & \left. + J_\mu^W \frac{\Lambda_b^{(-)}(k)}{\epsilon_b(k) + \epsilon_b(p_s)} \gamma_1^0 \mathcal{V}(\mathbf{p}_{\bar{s}} - \mathbf{q}_{\bar{s}}) \right\} u_b(q_b) u_s(q_{\bar{s}}), \end{aligned} \quad (10)$$

where  $\mathbf{k} = \mathbf{p}_s - \mathbf{\Delta}$ ;  $\mathbf{k}' = \mathbf{q}_b + \mathbf{\Delta}$ ;  $\mathbf{\Delta} = \mathbf{p}_f - \mathbf{p}_{B_s}$ ;

$$\Lambda^{(-)}(p) = \frac{\epsilon(p) - (m\gamma^0 + \gamma^0(\boldsymbol{\gamma}\mathbf{p}))}{2\epsilon(p)}, \quad \epsilon(p) = \sqrt{\mathbf{p}^2 + m^2}.$$

It depends in a very complicated way on the relative momenta of quarks which enter the energies of the initial heavy and final light quarks. For the heavy quark energy the heavy quark expansion can be applied. For the light quark such expansion is not valid. However, the final light  $f$  meson possesses a large recoil momentum ( $|\mathbf{\Delta}_{\max}| = (M_{B_s}^2 - M_f^2)/(2M_{B_s}) \sim 2.6$  GeV), with respect to the mean relative quark momentum  $|\mathbf{p}|$  in the meson ( $\sim 0.5$  GeV), almost in the whole kinematical range except the small region near  $q^2 = q_{\max}^2$  ( $|\mathbf{\Delta}| = 0$ ). This observation allows one to neglect  $|\mathbf{p}|$  compared to  $|\mathbf{\Delta}|$  in the light quark energy  $\epsilon_q(p + \mathbf{\Delta}) \equiv \sqrt{m_q^2 + (\mathbf{p} + \mathbf{\Delta})^2}$ , replacing it by  $\epsilon_q(\mathbf{\Delta}) \equiv \sqrt{m_q^2 + \mathbf{\Delta}^2}$  in expressions for the subleading contribution. Such replacement removes the relative momentum dependence in the energies of quarks and thus permits to perform one of the integrations in the subleading contribution using the quasipotential equation. Since the subleading contributions are additionally suppressed by the ratio of the small binding energy to the large total energy of the meson, the uncertainty introduced by such procedure is small. As the result the weak decay matrix element is expressed through the usual overlap integral of initial and final meson wave functions and its momentum dependence can be determined in the whole accessible kinematical range without additional assumptions.

It is important to point out that initial and final mesons in the considered rare decay are moving with respect to each other. This fact should be taken into account in calculating the decay matrix element (8). If calculations are done in the  $B_s$  meson rest frame ( $\mathbf{p}_{B_s} = 0$ ) then the final meson is moving with the recoil momentum  $\mathbf{p}_f = \mathbf{\Delta}$ . In the quasipotential approach the wave function of the moving meson  $\Psi_{f\mathbf{\Delta}}$  is connected with the wave function in the rest frame  $\Psi_{f\mathbf{0}} \equiv \Psi_f$  by the relativistic transformation [15]

$$\Psi_{f\mathbf{\Delta}}(\mathbf{p}) = D_s^{1/2}(R_{L\mathbf{\Delta}}^W)D_s^{1/2}(R_{L\mathbf{\Delta}}^W)\Psi_{f\mathbf{0}}(\mathbf{p}), \quad (11)$$

where  $R^W$  is the Wigner rotation,  $L_{\mathbf{\Delta}}$  is the Lorentz boost to a moving reference frame and  $D^{1/2}(R)$  is the spin rotation matrix.

### III. FORM FACTORS OF THE REAR WEAK TRANSITIONS OF $B_s$ TO $\eta(\varphi)$ MESONS

The matrix elements of the flavour changing neutral currents, governing rare  $b \rightarrow s$  weak transitions, between initial  $B_s$  meson and final  $\eta$  or  $\varphi$  mesons are usually parametrized by the following set of the invariant form factors

$$\langle \eta(p_\eta) | \bar{s}\gamma^\mu b | B_s(p_{B_s}) \rangle = f_+(q^2) \left[ p_{B_s}^\mu + p_\eta^\mu - \frac{M_{B_s}^2 - M_\eta^2}{q^2} q^\mu \right] + f_0(q^2) \frac{M_{B_s}^2 - M_\eta^2}{q^2} q^\mu, \quad (12)$$

$$\langle \eta(p_\eta) | \bar{s}\gamma^\mu \gamma_5 b | B_s(p_{B_s}) \rangle = 0, \quad (13)$$

$$\langle \eta(p_\eta) | \bar{s}\sigma^{\mu\nu} q_\nu b | B_s(p_{B_s}) \rangle = \frac{if_T(q^2)}{M_{B_s} + M_\eta} [q^2(p_{B_s}^\mu + p_\eta^\mu) - (M_{B_s}^2 - M_\eta^2)q^\mu], \quad (14)$$

$$\langle \varphi(p_\varphi) | \bar{s} \gamma^\mu b | B_s(p_{B_s}) \rangle = \frac{2iV(q^2)}{M_{B_s} + M_\varphi} \epsilon^{\mu\nu\rho\sigma} \epsilon_\nu^* p_{B_s\rho} p_{\varphi\sigma}, \quad (15)$$

$$\begin{aligned} \langle \varphi(p_\varphi) | \bar{s} \gamma^\mu \gamma_5 b | B_s(p_{B_s}) \rangle &= 2M_\varphi A_0(q^2) \frac{\epsilon^* \cdot q}{q^2} q^\mu + (M_{B_s} + M_\varphi) A_1(q^2) \left( \epsilon^{*\mu} - \frac{\epsilon^* \cdot q}{q^2} q^\mu \right) \\ &\quad - A_2(q^2) \frac{\epsilon^* \cdot q}{M_{B_s} + M_\varphi} \left[ p_{B_s}^\mu + p_\varphi^\mu - \frac{M_{B_s}^2 - M_\varphi^2}{q^2} q^\mu \right], \end{aligned} \quad (16)$$

$$\langle \varphi(p_\varphi) | \bar{s} i \sigma^{\mu\nu} q_\nu b | B_s(p_{B_s}) \rangle = 2T_1(q^2) \epsilon^{\mu\nu\rho\sigma} \epsilon_\nu^* p_{\varphi\rho} p_{B_s\sigma}, \quad (17)$$

$$\begin{aligned} \langle \varphi(p_\varphi) | \bar{s} i \sigma^{\mu\nu} \gamma_5 q_\nu b | B_s(p_{B_s}) \rangle &= T_2(q^2) [(M_{B_s}^2 - M_\varphi^2) \epsilon^{*\mu} - (\epsilon^* \cdot q) (p_{B_s}^\mu + p_\varphi^\mu)] \\ &\quad + T_3(q^2) (\epsilon^* \cdot q) \left[ q^\mu - \frac{q^2}{M_{B_s}^2 - M_\varphi^2} (p_{B_s}^\mu + p_\varphi^\mu) \right], \end{aligned} \quad (18)$$

were  $q = p_{B_s} - p_{\eta(\varphi)}$  is the momentum transfer,  $M_{B_s, \eta(\varphi)}$  are the initial and final meson masses, and  $\epsilon_\mu$  is the polarization vector of the final vector  $\varphi$  meson.

At the maximum recoil point ( $q^2 = 0$ ) these form factors satisfy the following conditions:

$$f_+(0) = f_0(0),$$

$$A_0(0) = \frac{M_{B_s} + M_\varphi}{2M_\varphi} A_1(0) - \frac{M_{B_s} - M_\varphi}{2M_\varphi} A_2(0),$$

$$T_1(0) = T_2(0).$$

The physical pseudoscalar  $\eta$  and  $\eta'$  mesons are the mixtures of  $\eta_q(u\bar{u} + d\bar{d})$  and  $\eta_s(s\bar{s})$  states

$$|\eta\rangle = |\eta_q\rangle \cos \phi - |\eta_s\rangle \sin \phi, \quad (19)$$

$$|\eta'\rangle = |\eta_q\rangle \sin \phi + |\eta_s\rangle \cos \phi. \quad (20)$$

For the calculations we use the experimental value of the mixing angle  $\phi = (41.4 \pm 0.3 \pm 0.7 \pm 0.6)^\circ$  [16] and neglect the possible glue content in these mesons. The wave functions of  $\eta_q$  and  $\eta_s$  mesons are known in our model from previous light meson mass spectra investigations [11]. The calculated masses of the pure  $\eta_q$  and  $\eta_s$  are  $M_{\eta_q} = 154$  MeV and  $M_{\eta_s} = 743$  MeV [11], while the masses of the mixed states  $\eta$  and  $\eta'$  are close to the experimental values.

Now we compare the form factor decompositions (12)–(18) with the results of the calculations of the weak current matrix element in our model, based on the methods described in the previous section. This allows us to explicitly determine the form factors in the whole accessible kinematical range through the overlap integrals of the meson wave functions. The corresponding expressions can be found in Refs. [9, 17]. For the numerical evaluations of the overlap integrals we use the quasipotential wave functions of  $B_s$  and  $\eta(\varphi)$  mesons previously obtained in their mass spectra studies [10, 11]. The calculated form factors are plotted in Figs. 3 and 4.

For the comparison of the obtained form factors with experiment and other theoretical calculations it is important to have approximate analytic expressions for them. Our analysis shows that the weak  $B_s \rightarrow \eta(\varphi)$  transition form factors can be well fitted by the following formulas [18, 19]:

TABLE I: Calculated form factors of weak  $B_s \rightarrow \eta_s$  and  $B_s \rightarrow \varphi$  transitions. Form factors  $f_+(q^2)$ ,  $f_T(q^2)$ ,  $V(q^2)$ ,  $A_0(q^2)$ ,  $T_1(q^2)$  are fitted by Eq. (21), and form factors  $f_0(q^2)$ ,  $A_1(q^2)$ ,  $A_2(q^2)$ ,  $T_2(q^2)$ ,  $T_3(q^2)$  are fitted by Eq. (22).

	$B_s \rightarrow \eta_s$			$B_s \rightarrow \varphi$						
	$f_+$	$f_0$	$f_T$	$V$	$A_0$	$A_1$	$A_2$	$T_1$	$T_2$	$T_3$
$F(0)$	0.384	0.384	0.301	0.406	0.322	0.320	0.318	0.275	0.275	0.133
$F(q_{\text{max}}^2)$	3.31	0.604	1.18	2.74	1.64	0.652	0.980	1.47	0.675	0.362
$\sigma_1$	-0.347	-0.120	-0.897	-0.861	-0.104	0.133	1.11	-0.491	0.396	0.639
$\sigma_2$	-1.55	-0.849	-1.34	-2.74	-1.19	-1.02	0.105	-1.90	-0.811	-0.531

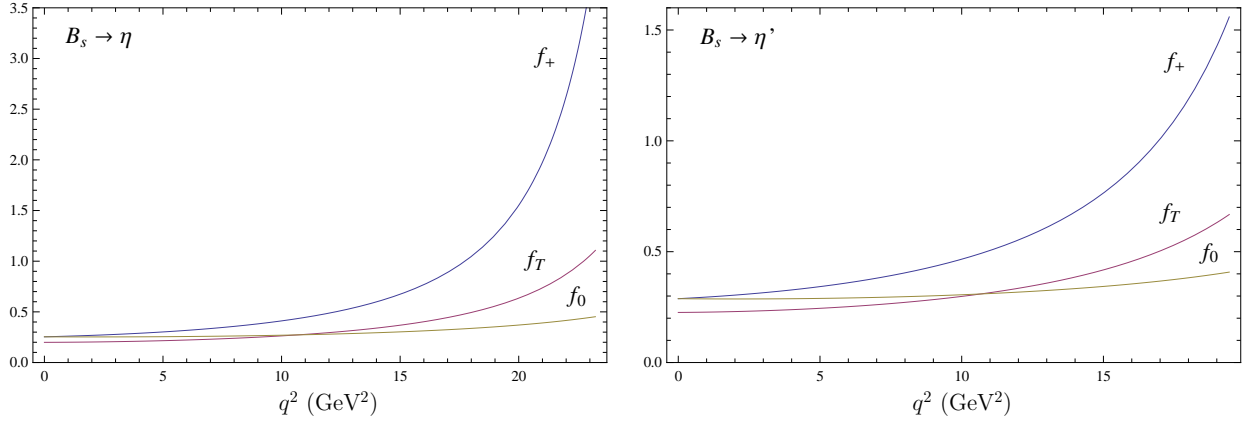


FIG. 3: Form factors of the weak  $B_s \rightarrow \eta$  and  $B_s \rightarrow \eta'$  transitions.

(a)  $F(q^2) = \{f_+(q^2), f_T(q^2), V(q^2), A_0(q^2), T_1(q^2)\}$

$$F(q^2) = \frac{F(0)}{\left(1 - \frac{q^2}{M^2}\right) \left(1 - \sigma_1 \frac{q^2}{M_{B_s^*}^2} + \sigma_2 \frac{q^4}{M_{B_s^*}^4}\right)}, \quad (21)$$

(b)  $F(q^2) = \{f_0(q^2), A_1(q^2), A_2(q^2), T_2(q^2), T_3(q^2)\}$

$$F(q^2) = \frac{F(0)}{\left(1 - \sigma_1 \frac{q^2}{M_{B_s^*}^2} + \sigma_2 \frac{q^4}{M_{B_s^*}^4}\right)}, \quad (22)$$

where  $M = M_{B_s^*}$  for the form factors  $f_+(q^2)$ ,  $f_T(q^2)$ ,  $V(q^2)$ ,  $T_1(q^2)$  and  $M = M_{B_s}$  for the form factor  $A_0(q^2)$ . The obtained values of  $F(0)$  and  $\sigma_{1,2}$  are given in Table I. The quality of such approximation is rather high, the deviation from the calculated form factors does not exceed 1%. The rough estimate of the total uncertainty of the form factors within our model gives its values of order of 5%. The subleading contributions (10) to the decay matrix elements in the region of small recoils are the main source of these uncertainties.

In Table II we confront our predictions for the form factors of rare weak  $B_s \rightarrow \eta_s$  and  $B_s \rightarrow \varphi$  transitions at maximum recoil ( $q^2 = 0$ ) with previous calculations [19–27] within various theoretical approaches. The different versions of light-cone sum rules are used in Refs. [20,

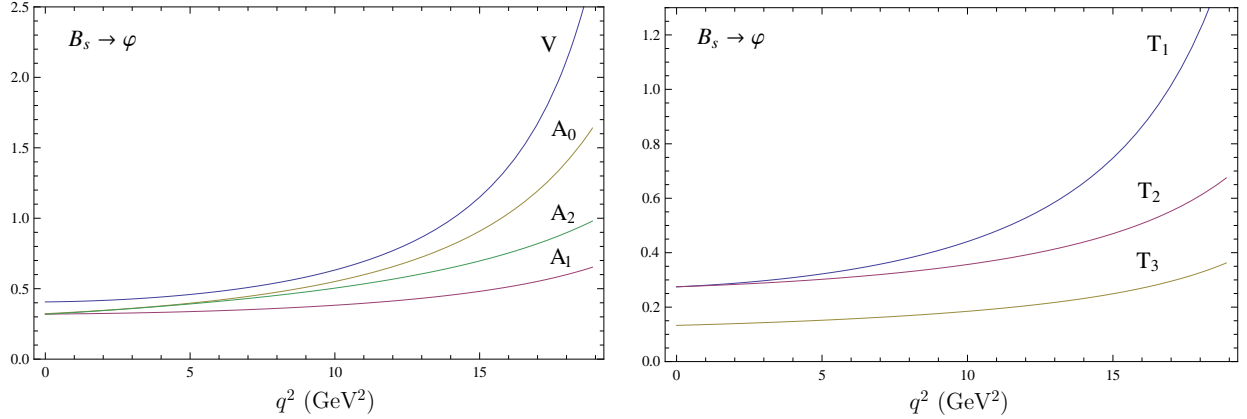


FIG. 4: Form factors of the weak  $B_s \rightarrow \varphi$  transitions.

25]. The authors of Refs. [21, 23] employ the perturbative QCD approach, while the covariant constituent quark model with the infrared confinement is used in Ref. [22]. Considerations in Ref. [19] are based on the constituent quark model and relativistic dispersion approach. The light-cone quark model calculations are performed in Refs. [24, 26] and the six-quark effective Hamiltonian model is employed in Ref. [27]. Comparison of the results presented in this table shows that, although there are some differences between predictions, in general there is a reasonable agreement between the values of these form factors at zero recoil calculated using significantly different theoretical methods. However, most of the discussed approaches allow the form factor calculation at the single point only or in some limited region of the recoil momentum, then some model extrapolation to the whole kinematical range should be used. The important advantage of our model is the explicit determination of the momentum dependence of the form factors without any additional assumptions.

Recently in Ref. [28] the method of extracting the  $B \rightarrow K^*$  transition form factors from available experimental data was proposed. It allows one to extract the ratios of the form factors  $V(q^2)/A_1(q^2)$  and  $A_1(q^2)/A_2(q^2)$  from the experimental data on angular distributions in this decay. Similar approach can be, in principle, applied for the  $B_s \rightarrow \varphi$  transition. In Fig. 5 we give our predictions for the corresponding form factor ratios. Using  $SU(3)$  symmetry arguments one can expect that the ratios of these form factors should have similar  $q^2$  behaviour for  $B$  and  $B_s$  decays. Indeed, we observe the qualitative agreement of these ratios with the ones found in Ref. [28].

In the following sections we apply the calculated form factors for the consideration of the rare semileptonic, radiative and nonleptonic decays of  $B_s$  mesons.

#### IV. RARE SEMILEPTONIC $B_s \rightarrow \eta(\varphi)l^+l^-$ DECAYS

First we consider the rare semileptonic decays. In the following calculations the usual factorization of short-distance (described by Wilson coefficients) and long-distance (which matrix elements are proportional to hadronic form factors) contributions in the effective Hamiltonian for the  $b \rightarrow s$  transitions is employed [29]

$$\mathcal{H}_{\text{eff}} = -\frac{4G_F}{\sqrt{2}}V_{ts}^*V_{tb}\sum_{i=1}^{10}c_i\mathcal{O}_i, \quad (23)$$



TABLE II: Comparison of theoretical predictions for the form factors of weak  $B_s \rightarrow \eta_s$  and  $B_s \rightarrow \varphi$  transitions at maximum recoil point  $q^2 = 0$ .

	$f_+(0)$	$f_T(0)$	$V(0)$	$A_0(0)$	$A_1(0)$	$A_2(0)$	$T_1(0)$	$T_3(0)$
This paper	$0.384 \pm 0.019$	$0.301 \pm 0.015$	$0.406 \pm 0.020$	$0.322 \pm 0.016$	$0.320 \pm 0.016$	$0.318 \pm 0.016$	$0.275 \pm 0.014$	$0.133 \pm 0.006$
[20]			$0.434 \pm 0.035$	$0.474 \pm 0.033$	$0.311 \pm 0.030$	$0.234 \pm 0.028$	$0.349 \pm 0.033$	$0.175 \pm 0.018$
[21]	$0.36 \pm 0.07$		$0.25 \pm 0.05$	$0.30 \pm 0.06$	$0.19 \pm 0.04$			
[22]			0.32		0.29	0.28	0.28	
[19]	0.36	0.36	0.44	0.42	0.34	0.31	0.38	0.26
[23]			$0.26 \pm 0.07$	$0.31^{+0.08}_{-0.07}$	$0.18^{+0.06}_{-0.05}$	$0.12 \pm 0.03$	$0.23^{+0.06}_{-0.05}$	$0.19^{+0.06}_{-0.05}$
[24]	0.288		0.329	0.279	0.232	0.210	0.276	0.170
[25]	$0.281 \pm 0.015$	$0.282 \pm 0.016$	$0.339 \pm 0.017$	$0.269 \pm 0.014$	$0.271 \pm 0.014$	$0.212 \pm 0.011$	$0.299 \pm 0.016$	$0.191 \pm 0.010$
[26]	0.357	0.365	0.445		0.343	0.310	0.380	
[27]			$0.259^{+0.082}_{-0.037}$	$0.311^{+0.098}_{-0.049}$	$0.194^{+0.054}_{-0.029}$			

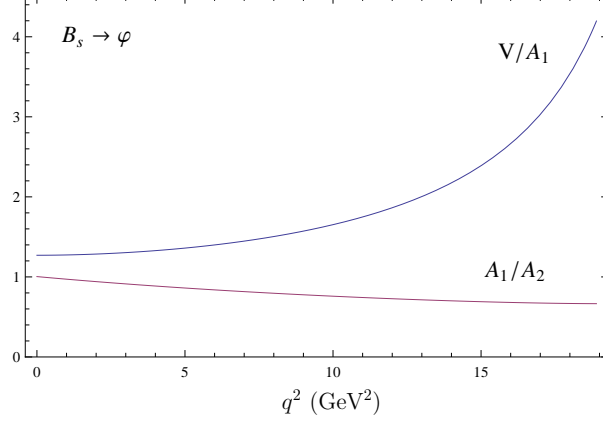


FIG. 5: The form factor ratios for the weak  $B_s \rightarrow \varphi$  transitions.

where  $G_F$  is the Fermi constant,  $V_{tj}$  are Cabibbo-Kobayashi-Maskawa matrix elements,  $c_i$  are the Wilson coefficients and  $\mathcal{O}_i$  are the standard model operators.

Then the matrix element of the  $b \rightarrow sl^+l^-$  transition amplitude between meson states can be written [30, 31] in the following form

$$\begin{aligned}\mathcal{M}(B_s \rightarrow \eta l^+ l^-) &= \frac{G_F \alpha}{2\sqrt{2}\pi} |V_{ts}^* V_{tb}| \left[ T_\mu^{(1)} (\bar{l} \gamma^\mu l) + T_\mu^{(2)} (\bar{l} \gamma^\mu \gamma_5 l) \right], \\ \mathcal{M}(B_s \rightarrow \varphi l^+ l^-) &= \frac{G_F \alpha}{2\sqrt{2}\pi} |V_{ts}^* V_{tb}| \left[ \epsilon^{\dagger\nu} T_{\mu\nu}^{(1)} (\bar{l} \gamma^\mu l) + \epsilon^{\dagger\nu} T_{\mu\nu}^{(2)} (\bar{l} \gamma^\mu \gamma_5 l) \right],\end{aligned}\quad (24)$$

where  $T^{(i)}$  are expressed through the form factors and the Wilson coefficients. These amplitudes can be written in the helicity basis  $\varepsilon^\mu(m)$  as follows (see [30])

(a)  $B \rightarrow \eta^{(\prime)}$  transition:

$$H_m^{(i)} = \varepsilon^{\dagger\mu}(m) T_\mu^{(i)}, \quad (25)$$

where

$$\begin{aligned}H_\pm^{(i)} &= 0, \\ H_0^{(1)} &= \frac{\lambda^{1/2}}{\sqrt{q^2}} \left[ c_9^{eff} f_+(q^2) + c_7^{eff} \frac{2m_b}{M_{B_s} + M_\eta} f_T(q^2) \right], \\ H_0^{(2)} &= \frac{\lambda^{1/2}}{\sqrt{q^2}} c_{10} f_+(q^2), \\ H_t^{(1)} &= \frac{M_{B_s}^2 - M_\eta^2}{\sqrt{q^2}} c_9^{eff} f_0(q^2), \\ H_t^{(2)} &= \frac{M_{B_s}^2 - M_\eta^2}{\sqrt{q^2}} c_{10} f_0(q^2).\end{aligned}\quad (26)$$

Here  $\lambda \equiv \lambda(M_{B_s}^2, M_F^2, q^2) = M_{B_s}^4 + M_F^4 + q^4 - 2(M_{B_s}^2 M_F^2 + M_F^2 q^2 + M_{B_s}^2 q^2)$  and the subscripts  $\pm, 0, t$  denote transverse, longitudinal and time helicity components, respectively.

(b)  $B \rightarrow \varphi$  transition:

$$H_m^{(i)} = \varepsilon^{\dagger\mu}(m) \epsilon^{\dagger\nu} T_{\mu\nu}^{(i)}, \quad (27)$$

where  $\epsilon^\nu$  is the polarization vector of the vector  $\varphi$  meson and

$$H_\pm^{(1)} = -(M_{B_s}^2 - M_\varphi^2) \left[ c_9^{eff} \frac{A_1(q^2)}{M_{B_s} - M_\varphi} + \frac{2m_b}{q^2} c_7^{eff} T_2(q^2) \right]$$

$$\begin{aligned}
& \pm \lambda^{1/2} \left[ c_9^{eff} \frac{V(q^2)}{M_{B_s} + M_\varphi} + \frac{2m_b}{q^2} c_7^{eff} T_1(q^2) \right], \\
H_\pm^{(2)} &= c_{10} \left[ -(M_{B_s} + M_\varphi) A_1(q^2) \pm \lambda^{1/2} \frac{V(q^2)}{M_B + M_\varphi} \right], \\
H_0^{(1)} &= -\frac{1}{2M_\varphi \sqrt{q^2}} \left[ c_9^{eff} \left\{ (M_{B_s}^2 - M_\varphi^2 - q^2)(M_{B_s} + M_\varphi) A_1(q^2) - \frac{\lambda}{M_{B_s} + M_\varphi} A_2(q^2) \right\} \right. \\
& \quad \left. + 2m_b c_7^{eff} \left\{ (M_{B_s}^2 + 3M_\varphi^2 - q^2) T_2(q^2) - \frac{\lambda}{M_{B_s}^2 - M_\varphi^2} T_3(q^2) \right\} \right], \\
H_0^{(2)} &= -\frac{1}{2M_V \sqrt{q^2}} c_{10} \left[ (M_{B_s}^2 - M_\varphi^2 - q^2)(M_{B_s} + M_\varphi) A_1(q^2) - \frac{\lambda}{M_{B_s} + M_\varphi} A_2(q^2) \right], \\
H_t^{(1)} &= -\frac{\lambda^{1/2}}{\sqrt{q^2}} c_9^{eff} A_0(q^2), \\
H_t^{(2)} &= -\frac{\lambda^{1/2}}{\sqrt{q^2}} c_{10} A_0(q^2). \tag{28}
\end{aligned}$$

The values of the Wilson coefficients  $c_i$  and of the effective Wilson coefficient  $c_7^{eff}$  are taken from Ref. [32]. The effective Wilson coefficient  $c_9^{eff}$  contains additional perturbative and long-distance contributions

$$c_9^{eff} = c_9 + \mathcal{Y}_{\text{pert}}(q^2) + \mathcal{Y}_{\text{BW}}(q^2). \tag{29}$$

The perturbative part is equal to

$$\begin{aligned}
\mathcal{Y}_{\text{pert}}(q^2) &= h\left(\frac{m_c}{m_b}, \frac{q^2}{m_b^2}\right) (3c_1 + c_2 + 3c_3 + c_4 + 3c_5 + c_6) \\
&\quad - \frac{1}{2} h\left(1, \frac{q^2}{m_b^2}\right) (4c_3 + 4c_4 + 3c_5 + c_6) \\
&\quad - \frac{1}{2} h\left(0, \frac{q^2}{m_b^2}\right) (c_3 + 3c_4) + \frac{2}{9} (3c_3 + c_4 + 3c_5 + c_6), \tag{30}
\end{aligned}$$

where

$$\begin{aligned}
h\left(\frac{m_c}{m_b}, \frac{q^2}{m_b^2}\right) &= -\frac{8}{9} \ln \frac{m_c}{m_b} + \frac{8}{27} + \frac{4}{9} x - \frac{2}{9} (2+x) |1-x|^{1/2} \begin{cases} \ln \left| \frac{\sqrt{1-x}+1}{\sqrt{1-x}-1} \right| - i\pi, & x \equiv \frac{4m_c^2}{q^2} < 1, \\ 2 \arctan \frac{1}{\sqrt{x-1}}, & x \equiv \frac{4m_c^2}{q^2} > 1, \end{cases} \\
h\left(0, \frac{q^2}{m_b^2}\right) &= \frac{8}{27} - \frac{4}{9} \ln \frac{q^2}{m_b^2} + \frac{4}{9} i\pi.
\end{aligned}$$

The long-distance (nonperturbative) contributions are assumed to originate from the  $c\bar{c}$  resonances ( $J/\psi, \psi' \dots$ ) and have a usual Breit-Wigner structure:

$$\mathcal{Y}_{\text{BW}}(q^2) = \frac{3\pi}{\alpha^2} \sum_{V_i=J/\psi, \psi(2S) \dots} \frac{\Gamma(V_i \rightarrow l^+ l^-) M_{V_i}}{M_{V_i}^2 - q^2 - i M_{V_i} \Gamma_{V_i}}. \tag{31}$$

We include contributions of the vector  $V_i(1^{--})$  charmonium states:  $J/\psi$ ,  $\psi(2S)$ ,  $\psi(3770)$ ,  $\psi(4040)$ ,  $\psi(4160)$  and  $\psi(4415)$ , with their masses ( $M_{V_i}$ ), leptonic  $[\Gamma(V_i \rightarrow l^+ l^-)]$  and total ( $\Gamma_{V_i}$ ) decay widths taken from PDG [1].

The differential decay rate can be written in terms of the helicity amplitudes [30] as follows

$$\begin{aligned} \frac{d\Gamma(B_s \rightarrow \eta(\varphi)l^+l^-)}{dq^2} &= \frac{G_F^2}{(2\pi)^3} \left( \frac{\alpha|V_{ts}^*V_{tb}|}{2\pi} \right)^2 \frac{\lambda^{1/2}q^2}{48M_{B_s}^3} \sqrt{1 - \frac{4m_l^2}{q^2}} \left[ H^{(1)}H^{\dagger(1)} \left( 1 + \frac{2m_l^2}{q^2} \right) \right. \\ &\quad \left. + H^{(2)}H^{\dagger(2)} \left( 1 - \frac{4m_l^2}{q^2} \right) + \frac{2m_l^2}{q^2} 3H_t^{(2)}H_t^{\dagger(2)} \right], \end{aligned} \quad (32)$$

where  $m_l$  is the lepton mass and

$$H^{(i)}H^{\dagger(i)} \equiv H_+^{(i)}H_+^{\dagger(i)} + H_-^{(i)}H_-^{\dagger(i)} + H_0^{(i)}H_0^{\dagger(i)}. \quad (33)$$

The other convenient observables for the  $B_s \rightarrow \varphi\mu^+\mu^-$  ( $\varphi \rightarrow K^+K^-$ ) decay, used in measurements, are the forward-backward asymmetry  $A_{FB}$  and the longitudinal fraction of the polarization of the vector  $\varphi$  meson  $F_L$ . They enter the differential decay distributions in  $\cos\theta_K$

$$\frac{1}{\Gamma} \frac{d\Gamma(B_s \rightarrow \varphi\mu^+\mu^-)}{d\cos\theta_K} = \frac{3}{2}F_L \cos^2\theta_K + \frac{3}{4}(1 - F_L)(1 - \cos^2\theta_K), \quad (34)$$

and in  $\cos\theta_\mu$

$$\frac{1}{\Gamma} \frac{d\Gamma(B_s \rightarrow \varphi\mu^+\mu^-)}{d\cos\theta_\mu} = \frac{3}{4}F_L(1 - \cos^2\theta_\mu) + \frac{3}{8}(1 - F_L)(1 + \cos^2\theta_\mu) + A_{FB} \cos\theta_\mu, \quad (35)$$

where  $\theta_K$  is the angle between the  $K^+$  direction and the direction opposite to the  $B_s$  meson in the  $\varphi$  rest frame, and  $\theta_\mu$  is the angle between the  $\mu^+$  and the opposite of the  $B$  direction in the dilepton rest frame.

These observables are expressed through the helicity amplitudes in the following way.

(a) The forward-backward asymmetry

$$A_{FB} = \frac{3}{4} \sqrt{1 - \frac{4m_l^2}{q^2}} \frac{\text{Re}(H_+^{(1)}H_+^{\dagger(2)}) - \text{Re}(H_-^{(1)}H_-^{\dagger(2)})}{H^{(1)}H^{\dagger(1)} \left( 1 + \frac{2m_l^2}{q^2} \right) + H^{(2)}H^{\dagger(2)} \left( 1 - \frac{4m_l^2}{q^2} \right) + \frac{2m_l^2}{q^2} 3H_t^{(2)}H_t^{\dagger(2)}}. \quad (36)$$

(b) The longitudinal polarization fraction of the vector  $\varphi$  meson

$$F_L = \frac{H_0^{(1)}H_0^{\dagger(1)} \left( 1 + \frac{2m_l^2}{q^2} \right) + H_0^{(2)}H_0^{\dagger(2)} \left( 1 - \frac{4m_l^2}{q^2} \right) + \frac{2m_l^2}{q^2} 3H_t^{(2)}H_t^{\dagger(2)}}{H^{(1)}H^{\dagger(1)} \left( 1 + \frac{2m_l^2}{q^2} \right) + H^{(2)}H^{\dagger(2)} \left( 1 - \frac{4m_l^2}{q^2} \right) + \frac{2m_l^2}{q^2} 3H_t^{(2)}H_t^{\dagger(2)}}. \quad (37)$$

They are the most popular quantities for the rare weak decays, since they can be determined experimentally using the angular analysis.

Now we substitute into these expressions the rare  $B_s$  decay form factors calculated in the previous section and obtain predictions of our model for the differential branching fractions, forward-backward asymmetry and longitudinal polarization fraction. They are plotted in Figs. 6–8. By solid lines we show results for the nonresonant branching fractions, where long-distance contributions (31) of the charmonium resonances to the coefficient  $c_9^{\text{eff}}$  are neglected. Plots given by the dashed lines contain such resonant contributions. For decays with the muon pair two largest peaks correspond to the contributions coming from the

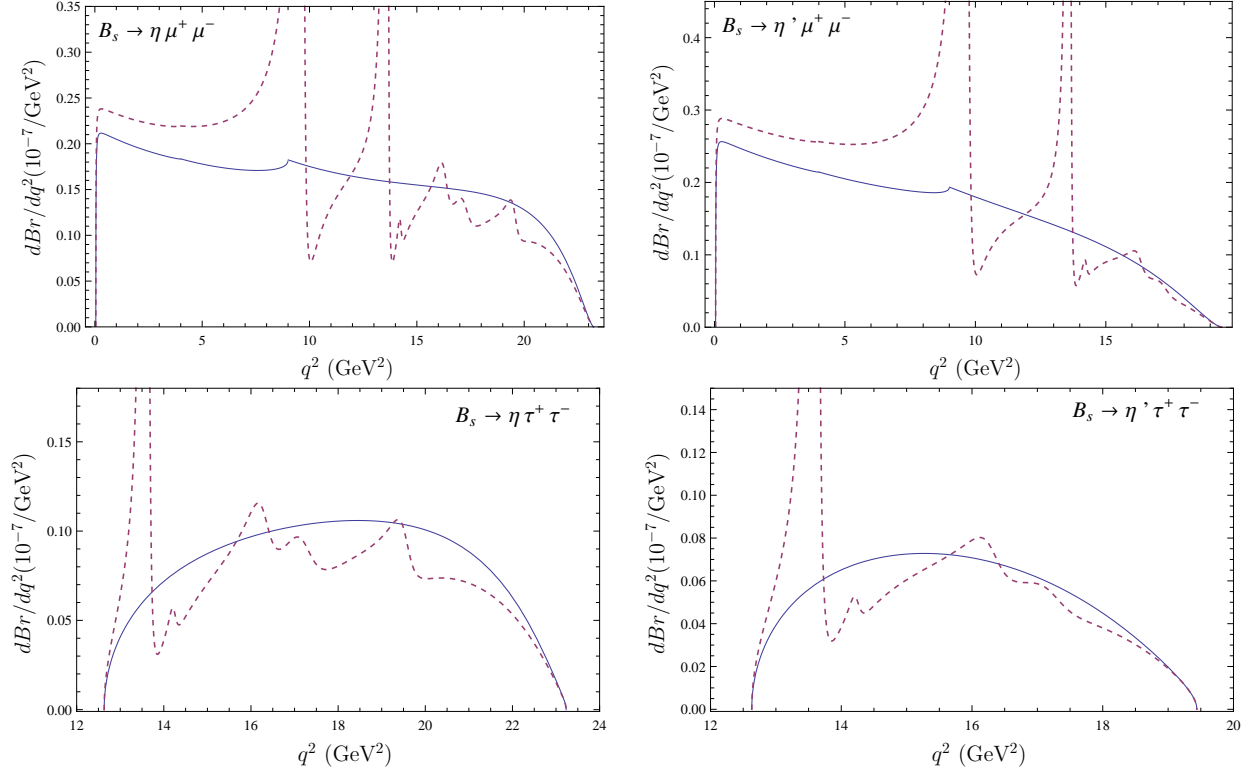


FIG. 6: Theoretical predictions for the differential branching fractions  $dBr(B_s \rightarrow \eta^{(\prime)} l^+ l^-)/dq^2$ . Nonresonant and resonant results are plotted by solid and dashed lines, respectively.

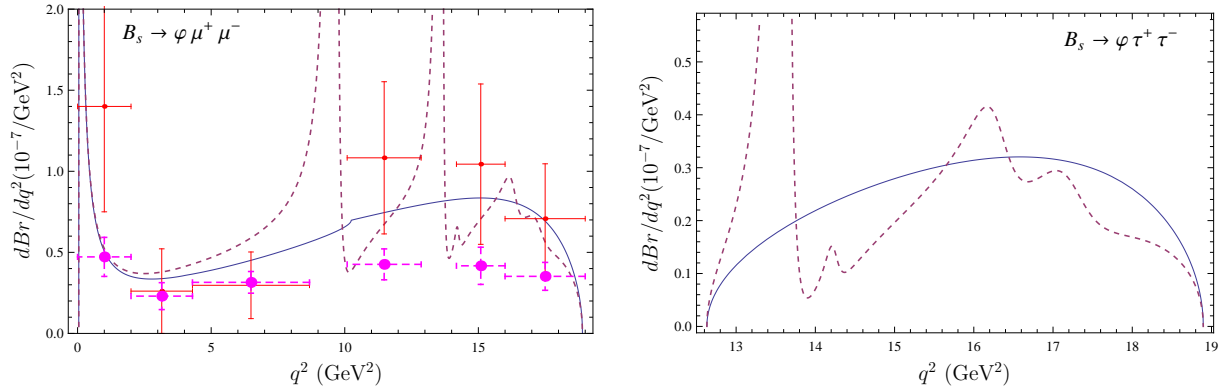


FIG. 7: Comparison of theoretical predictions for the differential branching fractions  $dBr(B_s \rightarrow \varphi \mu^+ \mu^-)/dq^2$  with available experimental data. Nonresonant and resonant results are plotted by solid and dashed lines, respectively. CDF data are given by dots with solid error bars, while LHCb data are presented by filled circles with dashed error bars.

lowest vector charmonium states  $J/\psi$  and  $\psi(2S)$ , since they are narrow. The region of these resonance peaks is excluded in experimental studies of these decays. Contributions in the low recoil region originating from the higher vector charmonium states, which are above the open charm threshold, are significantly less pronounced. Note that very recently the LHCb Collaboration observed a charmonium resonance in the similar rare decay  $B \rightarrow K \mu^+ \mu^-$  at

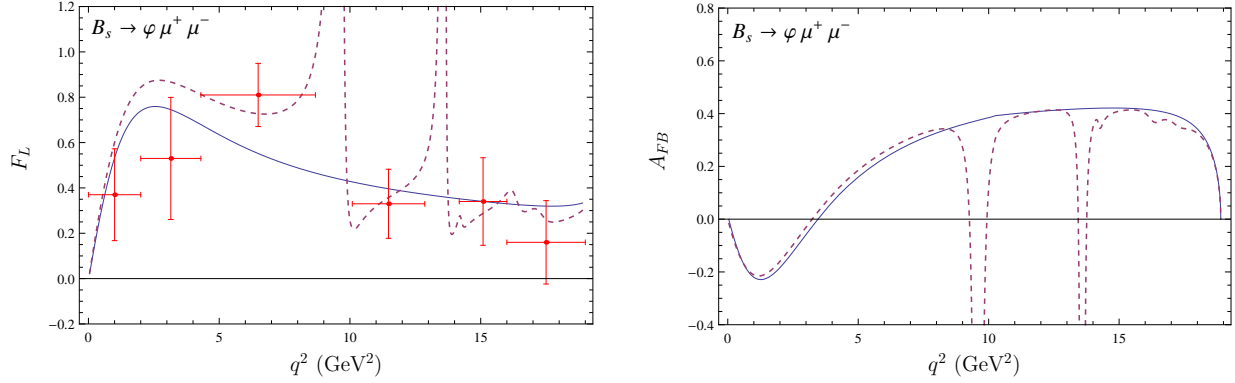


FIG. 8: Comparison of theoretical predictions for the  $\varphi$  longitudinal polarization  $F_L$  and muon forward-backward asymmetry  $A_{FB}$  for the rare  $B_s \rightarrow \varphi \mu^+ \mu^-$  decays with available experimental data. Nonresonant and resonant results are plotted by solid and dashed lines, respectively. LHCb data are given by dots with solid error bars.

TABLE III: Comparison of our predictions for the branching fractions of the rare semileptonic  $B_s \rightarrow \varphi \mu^+ \mu^-$  decays in several bins of  $q^2$  with experimental data (in  $10^{-7}$ ).

$q^2$ bin (GeV <sup>2</sup> )	Theory		Experiment	
	nonresonant	resonant	PDG [1]	LHCb [2]
$0.10 < q^2 < 2.00$	$1.4 \pm 0.2$	$1.4 \pm 0.2$	$2.8 \pm 1.3$	$0.944 \pm 0.241$
$2.00 < q^2 < 4.30$	$0.73 \pm 0.08$	$0.80 \pm 0.09$	$0.6 \pm 0.6$	$0.529 \pm 0.191$
$4.30 < q^2 < 8.68$	$1.8 \pm 0.2$	$2.4 \pm 0.3$	$1.3 \pm 0.9$	$1.38 \pm 0.29$
$10.09 < q^2 < 12.86$	$1.9 \pm 0.2$	$1.6 \pm 0.2$	$3.0 \pm 1.3$	$1.18 \pm 0.26$
$14.18 < q^2 < 16.00$	$1.4 \pm 0.2$	$1.2 \pm 0.2$	$1.9 \pm 0.9$	$0.759 \pm 0.209$
$16.00 < q^2$	$1.7 \pm 0.2$	$1.5 \pm 0.2$	$2.3 \pm 1.1$	$1.06 \pm 0.26$
$1.00 < q^2 < 6.00$	$1.7 \pm 0.2$	$1.9 \pm 0.2$	$1.1 \pm 0.9$	$1.14 \pm 0.28$
$0.10 < q^2 < 4.30$	$2.1 \pm 0.2$	$2.2 \pm 0.2$	$3.3 \pm 1.5$	$1.47 \pm 0.23$

low recoil [33]. Experimental data are available only for  $B_s \rightarrow \varphi \mu^+ \mu^-$  decays. In Figs. 7, 8 and in Tables III, IV we confront our predictions for differential branching fractions,  $dBr/dq^2$ , and the longitudinal polarization fraction,  $F_L$ , with experimental data from PDG (CDF) [1] and recent LHCb [2] data. The LHCb values for the differential branching fractions in most  $q^2$  bins are lower than the CDF ones, but experimental error bars are rather large. Our predictions lie just in between these experimental measurements. For the  $\varphi$  longitudinal polarization fraction,  $F_L$ , only LHCb data are available which agree with our results within uncertainties.

Now we integrate the differential branching fraction over  $q^2$  and get the results for the total branching fractions. For the evaluation of the branching fractions of the rare  $B_s \rightarrow K$  decays, governed by the  $b \rightarrow d$  weak current, we use the form factors previously calculated in our model in Ref. [8]. In Table V we present our predictions for the nonresonant branching fractions of the rare semileptonic  $B_s$  decays and compare them with previous calculations [25, 26, 34–36] and available experimental data [1, 2]. In Ref. [34] three sets of form factors based on different versions of sum rules were considered. Set A uses short-distance QCD sum

TABLE IV: Comparison of our predictions for the longitudinal polarization fraction  $F_L$  of the rare semileptonic  $B_s \rightarrow \varphi \mu^+ \mu^-$  decays in several bins of  $q^2$  with experimental data.

$q^2$ bin (GeV <sup>2</sup> )	Theory		Experiment
	nonresonant	resonant	LHCb [2]
$0.10 < q^2 < 2.00$	$0.50 \pm 0.05$	$0.56 \pm 0.06$	$0.37^{+0.20}_{-0.18}$
$2.00 < q^2 < 4.30$	$0.73 \pm 0.07$	$0.85 \pm 0.09$	$0.53^{+0.27}_{-0.25}$
$4.30 < q^2 < 8.68$	$0.54 \pm 0.05$	$0.77 \pm 0.08$	$0.81^{+0.12}_{-0.14}$
$10.09 < q^2 < 12.86$	$0.40 \pm 0.04$	$0.35 \pm 0.04$	$0.33^{+0.15}_{-0.13}$
$14.18 < q^2 < 16.00$	$0.34 \pm 0.03$	$0.29 \pm 0.03$	$0.34^{+0.19}_{-0.18}$
$16.00 < q^2 < 19.00$	$0.31 \pm 0.03$	$0.28 \pm 0.03$	$0.16^{+0.18}_{-0.12}$
$1.00 < q^2 < 6.00$	$0.68 \pm 0.07$	$0.80 \pm 0.08$	$0.56^{+0.19}_{-0.18}$

rules. Set B is based on light-cone QCD sum rules, while set C arises from light-cone QCD sum rules within the soft collinear effective theory. The authors of Ref. [26] employ the light front and constituent quark models for the evaluation of the rare decay branching fractions. Three-point QCD sum rules are used for the analysis of the rare semileptonic  $B_s$  decays into  $\eta(\eta')$  and lepton pair in Ref. [35]. In Ref. [36] calculations are based on the light-front quark model, while light-cone sum rules in the framework of heavy quark effective field theory are applied in Ref. [25]. The analysis of the predictions given in Table V indicate that these significantly different approaches give close values of order  $10^{-7}$  for the rare semileptonic  $B_s \rightarrow \varphi(\eta^{(\prime)}) l^+ l^-$  decay branching fractions and of order  $10^{-8}$  for  $B_s \rightarrow K^{(*)} l^+ l^-$  decays. Experimental data are available for the branching fraction of the  $B_s \rightarrow \varphi \mu^+ \mu^-$  decay only. As we see from the table all theoretical predictions are well consistent with each other and experimental data for the  $B_s \rightarrow \varphi \mu^+ \mu^-$  decay from PDG [1]. Note that very recently the LHCb Collaboration [2] also reported measurement of this decay branching fraction which is somewhat lower than previous measurements. Our prediction is consistent with the latter value within  $2\sigma$ .

## V. $B_s \rightarrow \eta(\varphi) \nu \bar{\nu}$ DECAYS

The differential decay rate for the  $B_s \rightarrow \eta(\varphi) \nu \bar{\nu}$  decay is given by [30]

$$\frac{d\Gamma(B_s \rightarrow \eta(\varphi) \nu \bar{\nu})}{dq^2} = 3 \frac{G_F^2}{(2\pi)^3} \left( \frac{\alpha |V_{ts}^* V_{tb}|}{2\pi} \right)^2 \frac{\lambda^{1/2} q^2}{24 M_{B_s}^3} H^{(\nu)} H^{\dagger(\nu)}, \quad (38)$$

where the factor 3 originates from the sum over neutrino flavours,

$$H^{(\nu)} H^{\dagger(\nu)} \equiv H_+^{(\nu)} H_+^{\dagger(\nu)} + H_-^{(\nu)} H_-^{\dagger(\nu)} + H_0^{(\nu)} H_0^{\dagger(\nu)},$$

and the helicity amplitudes  $H_m^{(\nu)}$  are expressed through form factors by the following relations.

(a)  $B \rightarrow \eta^{(\prime)}$  transition:

$$\begin{aligned} H_{\pm}^{(\nu)} &= 0, \\ H_0^{(\nu)} &= \frac{\lambda^{1/2}}{\sqrt{q^2}} C_L^\nu f_+(q^2). \end{aligned} \quad (39)$$

TABLE V: Comparison of theoretical predictions for the nonresonant branching fractions of the rare semileptonic  $B_s$  decays and available experimental data (in  $10^{-7}$ ).

Decay	This paper	[34]			[26]	[35]	[36]	[25]	Experiment	
		A	B	C					PDG [1]	LHCb [2]
$B_s \rightarrow \eta \mu^+ \mu^-$	$3.6 \pm 0.4$	$1.2 \pm 0.3$	$2.6 \pm 0.7$	$3.4 \pm 1.8$	3.12	$2.30 \pm 0.97$	2.4	$1.2 \pm 0.12$		
$B_s \rightarrow \eta \tau^+ \tau^-$	$0.87 \pm 0.09$	$0.30 \pm 0.05$	$0.80 \pm 0.15$	$1.0 \pm 0.55$	0.67	$0.373 \pm 0.156$	0.58	$0.34 \pm 0.04$		
$B_s \rightarrow \eta \nu \bar{\nu}$	$23.1 \pm 2.3$	$9.5 \pm 2$	$22 \pm 7$	$29 \pm 15$	21.7	$13.5 \pm 5.6$	17			
$B_s \rightarrow \eta' \mu^+ \mu^-$	$3.1 \pm 0.3$	$1.1 \pm 0.3$	$2.2 \pm 0.6$	$2.8 \pm 1.5$	3.42	$2.24 \pm 0.94$	1.8			
$B_s \rightarrow \eta' \tau^+ \tau^-$	$0.37 \pm 0.04$	$0.155 \pm 0.03$	$0.385 \pm 0.075$	$0.47 \pm 0.25$	0.43	$0.280 \pm 0.118$	0.26			
$B_s \rightarrow \eta' \nu \bar{\nu}$	$19.7 \pm 2.0$	$9 \pm 2$	$19 \pm 5$	$24 \pm 13$	23.8	$13.3 \pm 5.5$	13			
$B_s \rightarrow \varphi \mu^+ \mu^-$	$11.1 \pm 1.1$				16.4			$11.8 \pm 1.1$	$12.3^{+4.0}_{-3.4}$	$7.07^{+0.97}_{-0.94}$
$B_s \rightarrow \varphi \tau^+ \tau^-$	$1.5 \pm 0.2$				1.51			$1.23 \pm 0.11$		
$B_s \rightarrow \varphi \nu \bar{\nu}$	$79.6 \pm 8.0$				116.5				$< 54000$	
$B_s \rightarrow K \mu^+ \mu^-$	$0.22 \pm 0.02$						0.14	$0.199 \pm 0.021$		
$B_s \rightarrow K \tau^+ \tau^-$	$0.055 \pm 0.006$						0.03	$0.074 \pm 0.007$		
$B_s \rightarrow K \nu \bar{\nu}$	$1.41 \pm 0.14$						1.01			
$B_s \rightarrow K^* \mu^+ \mu^-$	$0.42 \pm 0.04$							$0.38 \pm 0.03$		
$B_s \rightarrow K^* \tau^+ \tau^-$	$0.075 \pm 0.008$							$0.050 \pm 0.004$		
$B_s \rightarrow K^* \nu \bar{\nu}$	$3.0 \pm 0.3$									



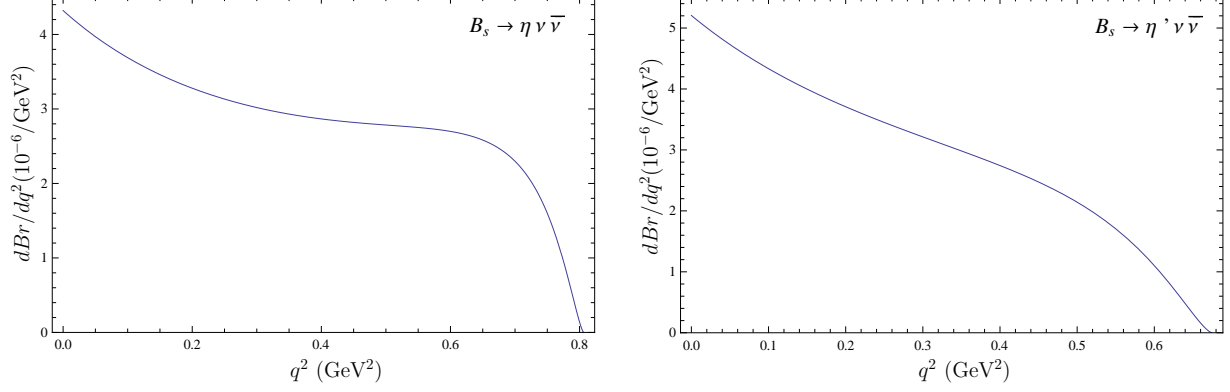


FIG. 9: Theoretical predictions for the differential branching fractions  $dBr(B_s \rightarrow \eta^{(\prime)} \nu \bar{\nu})/dq^2$ .

(b)  $B \rightarrow \varphi$  transition:

$$H_{\pm}^{(\nu)} = C_L^{\nu} \left[ -(M_{B_s} + M_{\varphi}) A_1(q^2) \pm \lambda^{1/2} \frac{V(q^2)}{M_{B_s} + M_{\varphi}} \right],$$

$$H_0^{(\nu)} = -\frac{1}{2M_{\varphi}\sqrt{q^2}} C_L^{\nu} \left[ (M_{B_s}^2 - M_{\varphi}^2 - q^2)(M_{B_s} + M_{\varphi}) A_1(q^2) - \frac{\lambda}{M_{B_s} + M_{\varphi}} A_2(q^2) \right]. \quad (40)$$

Here

$$C_L^{\nu} = -X(x_t)/\sin^2 \theta_W, \quad x_t = m_t^2/m_W^2,$$

$\theta_W$  is the Weinberg angle, and the function  $X(x_t)$  at the leading-order in QCD has the form

$$X(x_t) = \frac{x}{8} \left( \frac{2+x}{x-1} + \frac{3x-6}{(x-1)^2} \ln x \right),$$

while the next-to-leading order expressions are given in Ref. [37].

Substituting the experimental values for the top ( $m_t$ ) and  $W$ -boson ( $m_W$ ) masses one gets [38]

$$C_L^{\nu} = -6.38 \pm 0.06, \quad (41)$$

where the error is dominated by the top quark mass uncertainty. In the following calculations we use the central value of  $C_L^{\nu}$ .

The differential longitudinal polarization fraction  $F_L$  of the  $\varphi$  meson is defined similar to Eq. (37)

$$F_L = \frac{H_0^{(\nu)} H_0^{\dagger(\nu)}}{H^{(\nu)} H^{\dagger(\nu)}}. \quad (42)$$

Now we substitute the rare decay form factors calculated in our model into the above expressions for the branching fractions (38) and the longitudinal polarization fraction (42). The resulting predictions for the differential branching fractions of the  $B_s \rightarrow \eta(\eta') \nu \bar{\nu}$  decays are plotted in Fig. 9. In Fig. 10 we present the corresponding differential branching fraction and the  $\varphi$  longitudinal polarization fraction ( $F_L$ ) for the  $B_s \rightarrow \varphi \nu \bar{\nu}$  decay.

We give our results for the branching fractions of the rare  $B_s$  decays  $B_s \rightarrow \eta(\varphi) \nu \bar{\nu}$  and  $B_s \rightarrow K^{(*)} \nu \bar{\nu}$  in Table V in comparison with previous calculations [26, 34–36]. Again we find a reasonable agreement between predictions in significantly different approaches. The obtained branching fractions are of order  $10^{-6}$  for the  $B_s \rightarrow \eta(\varphi) \nu \bar{\nu}$  and  $10^{-7}$  for

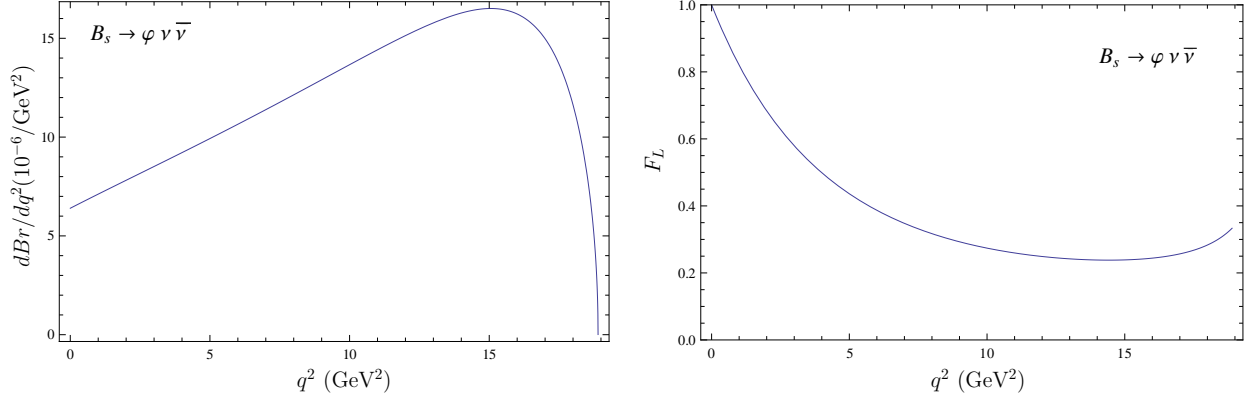


FIG. 10: Theoretical predictions for the differential branching fractions  $dBr(B_s \rightarrow \varphi \nu \bar{\nu})/dq^2$  and longitudinal polarization fraction  $F_L$  of the  $\varphi$  meson.

TABLE VI: Comparison of predictions for the branching fractions of the rare radiative decays with experimental data.

Decay	Theory		Experiment	
	This paper	[40]	PDG [1]	LHCb [4]
$Br(B^0 \rightarrow K^{*0} \gamma) \times 10^5$	$4.3 \pm 0.4$	$4.3 \pm 1.4$	$4.33 \pm 0.15$	
$Br(B_s \rightarrow \varphi \gamma) \times 10^5$	$3.8 \pm 0.4$	$4.3 \pm 1.4$	$5.7^{+2.2}_{-1.9}$	$3.5 \pm 0.4$
$\frac{Br(B^0 \rightarrow K^{*0} \gamma)}{Br(B_s \rightarrow \varphi \gamma)}$	$1.14 \pm 0.12$	$1.0 \pm 0.2$	$0.7 \pm 0.3$	$1.23 \pm 0.12$
$Br(B_s \rightarrow K^{*0} \gamma) \times 10^5$	$0.13 \pm 0.02$			

$B_s \rightarrow K^{(*)} \nu \bar{\nu}$  decay branching fractions. At present, only rather loose experimental upper bound (of order  $10^{-3}$ ) is available for the  $B_s \rightarrow \varphi \nu \bar{\nu}$  decay branching fraction. Of course, all predictions are well below this limit.

## VI. RARE RADIATIVE $B_s$ DECAYS

The exclusive rare radiative decay rate  $B_s \rightarrow \varphi \gamma$  for the emission of a real photon ( $k^2 = 0$ ) is determined by the form factor  $T_1(0)$  and is given by

$$\Gamma(B_s \rightarrow \varphi \gamma) = \frac{\alpha}{32\pi^4} G_F^2 m_b^2 M_{B_s}^3 |V_{tb} V_{ts}|^2 |c_7^{\text{eff}}(m_b)|^2 |T_1(0)|^2 \left(1 - \frac{M_\varphi^2}{M_{B_s}^2}\right)^3 \left(1 + \frac{M_\varphi^2}{M_{B_s}^2}\right). \quad (43)$$

To evaluate the rare radiative  $B_s \rightarrow \varphi \gamma$  decay rate we substitute the value of the form factor  $T_1(0)$  from Table I in the expression (43). The result is given in Table VI. There we also show our previous prediction for the  $Br(B^0 \rightarrow K^{*0} \gamma)$  [39]. In this table we confront our results with the values obtained in the framework of the soft collinear effective theory at NNLO [40] and available experimental data [1, 4]. We see that both theoretical predictions agree well with experimental values. We also compare results for the ratio of the rare radiative branching fractions of  $B$  and  $B_s$  decays. This ratio was recently measured with improved precision by the LHCb Collaboration [4]. The central value was found to be significantly larger than the previous one [1], but the errors are still large. Note that our

result is more close to the LHCb value but is consistent with both experimental values. In Table VI we also give our prediction for the still unmeasured CKM suppressed  $B_s \rightarrow K^{*0}\gamma$  decay.

## VII. RARE NONLEPTONIC $B_s$ DECAYS

Next we use the calculated form factors for the evaluation of the two-body nonleptonic decays of  $B_s$  mesons governed by the rare weak  $b \rightarrow s$  ( $b \rightarrow d$ ) transition. Following our previous calculations of the nonleptonic  $B_s$  decays [7, 8] we use the factorization approximation. As a result the complicated nonleptonic decay amplitude reduces to the product of the matrix element of the weak current between the  $B_s$  meson and the final  $\eta^{(\prime)}$  or  $\varphi$  meson with the matrix element of the weak current between the second meson and vacuum. For example the rare nonleptonic decay amplitude for  $B_s \rightarrow \eta^{(\prime)}\psi$  ( $\psi$  denotes the  $c\bar{c}$  meson) can be approximated by the product of the one-particle matrix elements

$$\langle \eta^{(\prime)}\psi | H_{\text{eff}} | B_s \rangle \approx \frac{G_F}{\sqrt{2}} V_{cb}^* V_{cs} a_2^{\text{eff}} \langle \eta^{(\prime)} | \bar{s}\gamma^\mu (1 - \gamma^5) b | B_s \rangle \langle \psi | (\bar{c}\gamma_\mu (1 - \gamma^5) c | 0 \rangle, \quad (44)$$

with the effective coefficient

$$a_2^{\text{eff}} = a_2 - \frac{V_{tb}^* V_{ts}}{V_{cb}^* V_{cs}} [a_3 + a_5 + a_7 + a_9] \approx a_2 + a_3 + a_5 + a_7 + a_9, \quad (45)$$

where terms in square brackets result from the contributions of penguin diagrams. In the right-hand-side of Eq. (45) we used the approximate relation,  $V_{tb}^* V_{ts} \approx -V_{cb}^* V_{cs}$ , following from the unitarity of the CKM matrix. The quantities  $a_{2n-1} = c_{2n-1} + c_{2n}/N_c$  and  $a_{2n} = c_{2n} + c_{2n-1}/N_c$  ( $n = 1, 2 \dots$  and  $N_c$  is the number of colors) are combinations of the Wilson coefficients  $c_i$ . The similar expressions can be obtained for other nonleptonic decays considered in this paper.

The matrix element of the weak current  $J_\mu^W$  between meson states is expressed through decay form factors calculated in Sec. III, while the matrix elements between vacuum and a final pseudoscalar ( $P$ ), vector ( $V$ ) or axial vector ( $A$ ) meson are parametrized by the decay constants  $f_{P,V,A}$

$$\begin{aligned} \langle P | \bar{q}_1 \gamma^\mu \gamma_5 q_2 | 0 \rangle &= i f_P p_P^\mu, \\ \langle V | \bar{q}_1 \gamma_\mu q_2 | 0 \rangle &= \epsilon_\mu M_V f_V, \\ \langle A | \bar{q}_1 \gamma^\mu \gamma_\mu q_2 | 0 \rangle &= \epsilon_\mu M_A f_A. \end{aligned} \quad (46)$$

For the calculations we use the following values of the decay constants:  $f_K = 0.156$  GeV,  $f_{K^*} = 0.214$  GeV,  $f_\varphi = 0.231$  GeV,  $f_{J/\psi} = 0.415$  GeV,  $f_{\chi_{c1}} = 0.161$  GeV, and the central values of the CKM matrix elements:  $|V_{cs}| = 0.973$ ,  $|V_{cb}| = 0.039$ ,  $|V_{td}| = 0.0087$ ,  $|V_{ts}| = 0.0404$ ,  $|V_{tb}| = 0.999$  [1].

In Table VII we compare our predictions for the rare nonleptonic  $B_s$  decays with other theoretical calculations [21, 22, 41–43] and available experimental data [1, 5, 6]. The authors of Ref. [41] analyze rare nonleptonic  $B_s$  decays to the ground or excited charmonium states and light mesons using generalized factorization and  $SU(3)$  symmetry to relate such modes to corresponding  $B$  decays. Nonleptonic  $B_s \rightarrow J/\psi \eta^{(\prime)}$  and  $B_s \rightarrow J/\psi \varphi$  decays are studied in Refs. [22, 42] in the framework of the covariant constituent quark model. Considerations of the rare nonleptonic  $B_s$  decays to light final mesons in Ref. [43] are based on

TABLE VII: Comparison of theoretical predictions for the branching fractions of the nonleptonic  $B_s$  decays with available experimental data (in  $10^{-4}$ ).

Decay	Theory				Experiment	
	this paper	[41]	[22, 42]	[43]	[21]	PDG [1] LHCb [5, 6]
$B_s \rightarrow J/\psi\eta$	$3.6 \pm 0.6$	$4.2 \pm 0.2$	4.67			$5.1^{+1.3}_{-1.0}$ $3.79^{+0.73}_{-0.80}$
$B_s \rightarrow J/\psi\eta'$	$3.7 \pm 0.6$	$4.3 \pm 0.2$	4.04			$3.7^{+1.0}_{-0.9}$ $3.42^{+0.66}_{-0.73}$
$B_s \rightarrow J/\psi\phi$	$11.3 \pm 1.6$	$16.7 \pm 5.7$	16			$10.9^{+2.8}_{-2.3}$ $10.5 \pm 1.05$
$B_s \rightarrow \psi(2S)\eta$	$1.9 \pm 0.3$	$3.0 \pm 0.2$				
$B_s \rightarrow \psi(2S)\eta'$	$1.6 \pm 0.3$	$2.5 \pm 0.2$				
$B_s \rightarrow \psi(2S)\phi$	$6.9 \pm 0.9$	$8.3 \pm 2.7$				$5.7^{+1.8}_{-1.6}$
$B_s \rightarrow \chi_{c1}\eta$	$0.56 \pm 0.09$	$2.0 \pm 0.2$				
$B_s \rightarrow \chi_{c1}\eta'$	$0.51 \pm 0.08$	$1.8 \pm 0.2$				
$B_s \rightarrow \chi_{c1}\phi$	$1.95 \pm 0.09$	$3.3 \pm 1.3$				
$B_s \rightarrow \phi\eta$	$0.018 \pm 0.003$			$0.0012^{+0.0139}_{-0.0023}$	$0.036^{+0.017}_{-0.012}$	
$B_s \rightarrow \phi\eta'$	$0.021 \pm 0.003$			$0.0005^{+0.0118}_{-0.0019}$	$0.0019^{+0.0020}_{-0.0013}$	
$B_s \rightarrow \phi\phi$	$0.22 \pm 0.03$			$0.218^{+0.304}_{-0.170}$	$0.353^{+0.187}_{-0.123}$	$0.19^{+0.06}_{-0.05}$
$B_s \rightarrow J/\psi K$	$0.25 \pm 0.05$					$0.36 \pm 0.08$
$B_s \rightarrow J/\psi K^*$	$0.57 \pm 0.09$					$0.9 \pm 0.4$
$B_s \rightarrow \psi(2S)K$	$0.12 \pm 0.02$					
$B_s \rightarrow \psi(2S)K^*$	$0.36 \pm 0.06$					
$B_s \rightarrow K^+K^-$	$0.19 \pm 0.03$			$0.227^{+0.275}_{-0.130}$	$0.136^{+0.086}_{-0.052}$	$0.264 \pm 0.028$
$B_s \rightarrow K^+K^{*-}$	$0.27 \pm 0.05$			$0.055^{+0.151}_{-0.047}$	$0.047^{+0.027}_{-0.016}$	
$B_s \rightarrow K^{*+}K^-$	$0.15 \pm 0.03$			$0.041^{+0.096}_{-0.032}$	$0.060^{+0.025}_{-0.020}$	
$B_s \rightarrow K^{*+}K^{*-}$	$0.29 \pm 0.05$			$0.091^{+0.105}_{-0.063}$	$0.067^{+0.039}_{-0.022}$	
$B_s \rightarrow K^0\bar{K}^0$	$0.15 \pm 0.03$			$0.247^{+0.293}_{-0.140}$	$0.156^{+0.097}_{-0.060}$	$< 0.66$
$B_s \rightarrow \bar{K}^0 K^{*0}$	$0.24 \pm 0.05$			$0.039^{+0.106}_{-0.035}$	$0.073^{+0.033}_{-0.022}$	
$B_s \rightarrow \bar{K}^{*0} K^0$	$0.13 \pm 0.03$			$0.042^{+0.140}_{-0.040}$	$0.043^{+0.023}_{-0.016}$	
$B_s \rightarrow K^{*0}\bar{K}^{*0}$	$0.26 \pm 0.05$			$0.091^{+0.113}_{-0.068}$	$0.078^{+0.043}_{-0.027}$	$0.28 \pm 0.07$
$B_s \rightarrow \phi\bar{K}^{*0}$	$0.0076 \pm 0.0012$			$0.004^{+0.005}_{-0.003}$	$0.0065^{+0.0033}_{-0.0023}$	$< 10$ $0.011 \pm 0.003$

QCD factorization, while perturbative QCD approach is adopted in Ref. [21]. Comparison of our predictions for the rare  $B_s$  decays to charmonium states and a light mesons with results of Refs. [22, 41, 42] shows that our model yields the central values 30-60% lower, especially for decays involving  $\chi_{c1}$ . However results are still compatible taking into account the uncertainties. They are also in agreement with the available experimental data, our central values for these decays being slightly closer to the experimental central values recently published by the LHCb Collaboration [5]. Very recently the Belle Collaboration [44] reported a measurement of the branching fraction of the decay  $B_s \rightarrow J/\psi\phi$  with the value  $Br(B_s \rightarrow J/\psi\phi) = (1.25 \pm 0.07 \pm 0.08 \pm 0.22) \times 10^{-3}$ . For the rare  $B_s$  decays to the pair of light mesons our predictions in general agree with results of Refs. [21, 43] and experiment taking into account rather large error bars. Note that very recently the LHCb Collaboration [6] reported the first observation of the decay  $B_s \rightarrow \phi\bar{K}^{*0}$ . The obtained central value of this decay branching fraction is found to be larger than theoretical expectations (our result

TABLE VIII: Comparison of theoretical predictions for the ratios of branching fractions of the nonleptonic  $B_s$  decays with experimental data.

Ratio	Theory			Experiment	
	this paper	[41]	[22, 42]	PDG [1]	LHCb [5]
$\frac{Br(B_s \rightarrow J/\psi \eta')}{Br(B_s \rightarrow J/\psi \eta)}$	$1.03 \pm 0.10$	$1.02 \pm 0.05$	0.87	$0.73 \pm 0.14$	$0.90^{+0.11}_{-0.09}$
$\frac{Br(B_s \rightarrow \psi(2S) \eta)}{Br(B_s \rightarrow J/\psi \eta)}$	$0.53 \pm 0.05$	$0.71 \pm 0.24$			$0.83 \pm 0.19$
$\frac{Br(B_s \rightarrow \psi(2S) \varphi)}{Br(B_s \rightarrow J/\psi \varphi)}$	$0.61 \pm 0.06$	$0.50 \pm 0.17$		$0.53 \pm 0.10$	
$\frac{Br(B_s \rightarrow \chi_{c1} \varphi)}{Br(B_s \rightarrow J/\psi \varphi)} \times 10^2$	$17.3 \pm 1.7$	$19.8 \pm 6.7$			$18.9 \pm 2.4$
$\frac{Br(B_s \rightarrow \varphi \mu^+ \mu^-)}{Br(B_s \rightarrow J/\psi \varphi)} \times 10^4$	$10.3 \pm 1.0$			$11.3 \pm 2.0$	$6.74 \pm 0.63$

is the closest to experiment) but the experimental and theoretical values agree within error bars.

In Table VIII we present comparison of predictions for the ratios of branching fractions of the rare nonleptonic  $B_s$  decays to the charmonium state and a light meson with experimental data which have smaller error bars. In general, good agreement of theory with experiment is observed. In this table we also give the ratio of the branching fractions of the rare semileptonic  $B_s \rightarrow \varphi \mu^+ \mu^-$  and nonleptonic  $B_s \rightarrow J/\psi \varphi$  decays. Our prediction is in accord with the PDG value [1], but almost a factor 1.5 larger than the recent LHCb value. This is the consequence of the significantly lower LHCb value for  $Br(B_s \rightarrow \varphi \mu^+ \mu^-)$  as it was already mentioned in Sec. IV.

## VIII. CONCLUSIONS

The form factors parametrizing the transition matrix element of the flavour changing neutral current, governed by  $b \rightarrow s$  quark transition, between the  $B_s$  and light ( $\eta(\eta')$  or  $\varphi$ ) mesons were calculated on the basis of the relativistic quark model with the QCD-motivated quark-antiquark interaction potential. All relativistic effects, including boosts of the meson wave functions and contributions of the intermediate negative-energy states, were consistently taken into account. The main advantage of the adopted approach consists in that it allows the determination of the momentum transfer dependence of the form factors in the whole accessible kinematical range. Therefore no additional assumptions and ad hoc extrapolations are needed for the description of the rare weak decay processes which have rather broad kinematical range. This significantly improves the reliability of the obtained results.

The calculated form factors were used while considering the rare semileptonic, radiative and nonleptonic  $B_s$  decays. The differential and total decay branching fractions as well as asymmetry and polarization parameters were evaluated. The obtained results were confronted with previous investigations based on significantly different theoretical approaches and available experimental data. Good agreement of our predictions with measured values is observed.

### Acknowledgments

The authors are grateful to A. Ali, D. Ebert, C. Hambrock, M. A. Ivanov, V. A. Matveev and V. I. Savrin for useful discussions. This work was supported in part by the *Russian Foundation for Basic Research* under Grant No.12-02-00053-a.

- 
- [1] J. Beringer *et al.* [Particle Data Group], Phys. Rev. D **86**, 010001 (2012).
  - [2] R. Aaij *et al.* [LHCb Collaboration], JHEP **1307**, 084 (2013).
  - [3] J. Li *et al.* [Belle Collaboration], Phys. Rev. Lett. **108**, 181808 (2012).
  - [4] R. Aaij *et al.* [LHCb Collaboration], Nucl. Phys. B **867**, 1 (2013).
  - [5] R. Aaij *et al.* [LHCb Collaboration], Nucl. Phys. B **867**, 547 (2013); , Phys. Rev. D **87**, 072004 (2013); Nucl. Phys. B **871**, 403 (2013); Nucl. Phys. B **874**, 663 (2013).
  - [6] R. Aaij *et al.* [LHCb Collaboration], arXiv:1306.2239 [hep-ex].
  - [7] R. N. Faustov and V. O. Galkin, Phys. Rev. D **87**, 034033 (2013).
  - [8] R. N. Faustov and V. O. Galkin, Phys. Rev. D **87**, 094028 (2013).
  - [9] D. Ebert, R. N. Faustov and V. O. Galkin, Phys. Rev. D **82**, 034032 (2010).
  - [10] D. Ebert, V. O. Galkin and R. N. Faustov, Phys. Rev. D **57**, 5663 (1998) [Erratum-ibid. D **59**, 019902 (1999)]; D. Ebert, R. N. Faustov and V. O. Galkin, Eur. Phys. J. C **66**, 197 (2010).
  - [11] D. Ebert, R. N. Faustov and V. O. Galkin, Phys. Rev. D **79**, 114029 (2009).
  - [12] D. Ebert, R. N. Faustov and V. O. Galkin, Phys. Rev. D **67**, 014027 (2003); Eur. Phys. J. C **71**, 1825 (2011).
  - [13] R. N. Faustov and V. O. Galkin, Z. Phys. C **66**, 119 (1995).
  - [14] D. Ebert, R. N. Faustov and V. O. Galkin, Phys. Rev. D **73**, 094002 (2006).
  - [15] R. N. Faustov, Ann. Phys. **78**, 176 (1973); Nuovo Cimento A **69**, 37 (1970).
  - [16] F. Ambrosino *et al.* [KLOE Collaboration], Phys. Lett. B **648**, 267 (2007).
  - [17] D. Ebert, R. N. Faustov and V. O. Galkin, Phys. Rev. D **82**, 034019 (2010).
  - [18] D. Ebert, R. N. Faustov and V. O. Galkin, Phys. Rev. D **75**, 074008 (2007).
  - [19] D. Melikhov and B. Stech, Phys. Rev. D **62**, 014006 (2000).
  - [20] P. Ball and R. Zwicky, Phys. Rev. D **71**, 014029 (2005).
  - [21] A. Ali, G. Kramer, Y. Li, C. -D. Lu, Y. -L. Shen, W. Wang and Y. -M. Wang, Phys. Rev. D **76**, 074018 (2007).
  - [22] M. A. Ivanov, J. G. Korner, S. G. Kovalenko, P. Santorelli and G. G. Saidullaeva, Phys. Rev. D **85**, 034004 (2012).
  - [23] R. -H. Li, C. -D. Lu and W. Wang, Phys. Rev. D **79**, 034014 (2009).
  - [24] C. -D. Lu, W. Wang and Z. -T. Wei, Phys. Rev. D **76**, 014013 (2007).
  - [25] Y. -L. Wu, M. Zhong and Y. -B. Zuo, Int. J. Mod. Phys. A **21**, 6125 (2006).
  - [26] C. Q. Geng and C. C. Liu, J. Phys. G **29**, 1103 (2003).
  - [27] F. Su, Y. -L. Wu, Y. -B. Yang and C. Zhuang, Eur. Phys. J. C **72**, 1914 (2012).
  - [28] C. Hambrock and G. Hiller, Phys. Rev. Lett. **109**, 091802 (2012).
  - [29] G. Buchalla, G. Hiller and G. Isidori, Phys. Rev. D **63**, 014015 (2000).
  - [30] A. Faessler, T. Gutsche, M. A. Ivanov, J. G. Körner and V. E. Lyubovitskij, Eur. Phys. J. direct C **4**, 18 (2002).
  - [31] A. Ali, P. Ball, L. T. Handoko and G. Hiller, Phys. Rev. D **61**, 074024 (2000).
  - [32] W. Altmannshofer, P. Ball, A. Bharucha, A. J. Buras, D. M. Straub and M. Wick, JHEP

- 0901**, 019 (2009).
- [33] R. Aaij *et al.* [LHCb Collaboration], arXiv:1307.7595 [hep-ex].
  - [34] M. V. Carlucci, P. Colangelo and F. De Fazio, Phys. Rev. D **80**, 055023 (2009).
  - [35] K. Azizi, R. Khosravi and F. Falahati, Phys. Rev. D **82**, 116001 (2010).
  - [36] H. -M. Choi, J. Phys. **37**, 085005 (2010).
  - [37] M. Misiak and J. Urban, Phys. Lett. B **451**, 161 (1999).
  - [38] W. Altmannshofer, A. J. Buras, D. M. Straub and M. Wick, JHEP **04**, 022 (2009).
  - [39] R. N. Faustov and V. O. Galkin, Phys. Rev. D **52**, 5131 (1995); D. Ebert, R. N. Faustov and V. O. Galkin, Phys. Rev. D **64**, 094022 (2001); D. Ebert, R. N. Faustov, V. O. Galkin and H. Toki, Phys. Rev. D **64**, 054001 (2001).
  - [40] A. Ali, B. D. Pecjak and C. Greub, Eur. Phys. J. C **55**, 577 (2008).
  - [41] P. Colangelo, F. De Fazio and W. Wang, Phys. Rev. D **83**, 094027 (2011).
  - [42] S. Dubnicka, A. Z. Dubnickova, M. A. Ivanov and A. Liptaj, Phys. Rev. D **87**, 074201 (2013).
  - [43] M. Beneke and M. Neubert, Nucl. Phys. B **675**, 333 (2003).
  - [44] F. Thorne *et al.* [Belle Collaboration], arXiv:1309.0704 [hep-ex].